

# A Geometrically Nonlinear Nine-Node Solid Shell Element Formulation with Reduced Sensitivity to Mesh Distortion

Keejoo Lee<sup>1</sup>, Chahngmin Cho<sup>2</sup>, and Sung W. Lee<sup>1</sup>

**Abstract:** A geometrically nonlinear assumed strain formulation is introduced in conjunction with bubble function displacements to improve the performance of a nine-node solid shell element. The assumed strain field has been carefully selected to avoid both element locking and undesirable spurious kinematic modes. The results of numerical tests demonstrate that the present approach leads to an element that is significantly less sensitive to mesh distortion than the existing element.

**keyword:** assumed strain formulation, solid shell element, geometrically nonlinear, and bubble function

## 1 Introduction

There has been considerable progress made in the finite element modeling of shells. For an extensive literature survey on shell finite elements, one may refer to Yang, Saigal, Masoud, and Kapania (2000). Depending upon whether it allows changes in the thickness, a shell formulation can be classified as either an ‘inextensible’ theory or an ‘extensible’ theory. One of the inextensible shell formulations is the degenerated solid shell approach [Ahmad, Irons, and Zienkiewicz (1970)], which has been popular in finite element modeling of both thick and thin shell structures. The kinematics of deformation is usually described by five degrees of freedom – three translations and two rotations. Simo and Rifai (1990) presented a formulation based on the exact finite rotation theory using the inextensibility assumption in the thickness direction. Among the shell element formulations based on the extensible theory, the simplest approach is to treat the shell as a three-dimensional solid. This solid shell element approach does not need rotational angles to describe the kinematics of deformation. Accordingly, all kinematic variables are expressed in vector forms, based

on a global coordinate system alone. Particularly, for geometrically nonlinear analysis, large load increments are possible with the solid shell approach [Park, Cho, and Lee (1995)]. For the solid shell approach, the constitutive law is constructed to incorporate physical behavior of thin shell structures [Ausserer and Lee (1988), Kim and Lee (1988)]. Also, alternate extensible theory formulations using stretchable directors through the thickness were introduced by Simo, Rifai, and Fox (1990), Andelfinger and Ramm (1993), Betsch and Stein (1995), and Buchter, Ramm, and Roehl (1994). These formulations allow large load increments in geometrically nonlinear analyses.

Both the inextensible and extensible theory shell elements based on the assumed displacement alone suffer from the element locking as the shell becomes thin. Element locking is caused by the over-constraining effect of zero strains on the assumed displacement field of an element. The effect of locking can become more pronounced when the kinematic constraints are combined with boundary conditions or distortion of the element geometry. Various methods such as reduced or selective integration schemes and assumed strain or stress formulations have been introduced to alleviate the element locking. Elements with excessively reduced integration schemes exhibit spurious kinematic modes that cannot be controlled. Accordingly, Lee and Pian (1978) introduced an approach, in which an independently assumed strain field can be selected to alleviate element locking without triggering spurious kinematic modes. Since then, other approaches such as the assumed strain or stress method, the direct assumed natural strain method and the enhanced assumed strain method have been presented. Several assumed strain/stress formulation shell elements, combined with the inextensible degenerated solid shell approach, were introduced by Rhiu and Lee (1987) and others [Rhiu, Russell and Lee (1990), Yeom and Lee (1989), Saleeb, Chang, Graf, and Yingyeunyoung (1990)]. Assumed strain formulation was combined

<sup>1</sup> Department of Aerospace Engineering, University of Maryland College Park, MD, U.S.A.

<sup>2</sup> Currently at ADD, Daejon, Korea

with the three-dimensional solid shell approach to develop shell elements for geometrically linear and nonlinear analyses [Ausserer and Lee (1988), Kim and Lee (1988), and Park and Lee (1995)]. In addition, alternate assumed strain formulations combined with the extensible director shell kinematics were presented by Simo, Rifai, and Fox (1990), Andelfinger and Ramm (1993), and Betsch and Stein (1995).

As an alternative approach to reduce element locking, the bubble function displacement has been combined with the assumed strain or stress formulation. For example, Pinsky and Jasti (1989) showed that the bubble function displacements combined with an assumed stress field improved element performance by eliminating transverse shear locking. Kemp, Cho, and Lee (1998) demonstrated that, even for elements of distorted geometry, locking of the four-node element could be alleviated using the simplest bubble functions combined with a carefully chosen assumed strain field. These studies were limited to geometrically linear plates and shells. Kim, Kim, and Lee (2000) and Hong, Kim, and Lee (2001) introduced bubble functions to construct triangular solid shell elements for both small and finite rotation problems.

It is well to mention that, in addition to Finite Element Method, there are other numerical techniques for analysis of thin structures such as the Meshless Method and the Boundary Element Method [El-Zafrany (2001)]. In the Meshless Method, approximate solutions are constructed based on a set of scattered nodes, instead of using elements with nodal degrees of freedom. There exist various versions of the Meshless Method, including Diffuse Element Method (DEM), Element-Free Galerkin (EFG) method, and Meshless Local Petrov-Galerkin method (MLPG). In particular, recent studies conducted by Cho, Kim, and Atluri (1999), Gu and Liu (2001), and Cho and Atluri (2001), have demonstrated that the MLPG method can be made locking-free and effective in the analysis of thin shell structures.

Although there has been considerable progress, there still exist room for improvement in the finite element modeling of shell structures undergoing geometrically linear and nonlinear deformations. Accordingly, the objective of this work is to develop a nine-node solid shell element with improved performance, especially when it is necessary to use elements of distorted geometry to model geometrically nonlinear shell structures. The present study is based on the solid shell approach that treats the shell

structure as a three-dimensional solid. The kinematics of deformation is described by six vector components at a point on the shell mid-surface. The bubble function displacements are added to the assumed displacements and eliminated at the element level. Special emphasis is placed on the proper selection of high-order assumed strain terms in conjunction with the bubble function displacements.

## 2 Finite Element Formulation

A geometrically nonlinear assumed strain solid shell element formulation is developed based on the total Lagrangian description that employs the Green strain and the second Piola-Kirchhoff stress.

### 2.1 Element geometry and kinematics of deformation

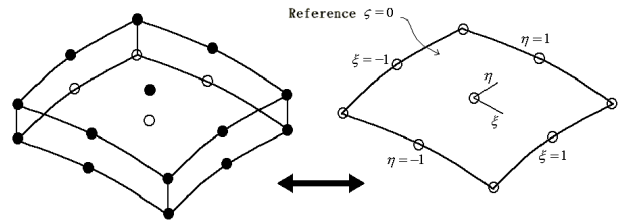


**Figure 1** : Two versions of the solid shell element, 18-node and 9-node versions

Figure 1 shows two versions of a solid shell element, one with eighteen nodes and the other with nine nodes. The eighteen-node version has three degrees of freedom per node while the nine-node version has six degrees of freedom per node. The two versions are equivalent to each other. For the nine-node version, the element geometry can be described as follows:

$$\mathbf{x} = \mathbf{x}_0 + \zeta \frac{t}{2} \mathbf{a}_3 = \sum_{i=1}^n N_i(\xi, \eta) (\mathbf{x}_0)_i + \zeta \sum_{i=1}^n N_i(\xi, \eta) \left( \frac{t}{2} \mathbf{a}_3 \right)_i \quad (1)$$

where  $\mathbf{x}_0$  is the position vector of a point on the shell mid-surface,  $\mathbf{a}_3$  is a unit vector in the thickness direction,  $n$  is the number of nodes on the mid-surface of an element,  $(\mathbf{x}_0)_i$  is a nodal position vector,  $N_i$  is the mapping function corresponding to the  $i$ -th node, and  $t$  is the shell thickness. In equation (1),  $\xi$ ,  $\eta$ , and  $\zeta$  are the parental coordinates with  $\zeta$  in the thickness direction.

The displacement vector  $\mathbf{u}$  can be expressed as follows:

$$\mathbf{u} = \mathbf{u}_9 + \mathbf{u}_b \quad (2)$$

In the above equation,  $\mathbf{u}_9$  is the assumed displacement vector corresponding to the nine-node interpolation, and  $\mathbf{u}_b$  is a bubble function displacement vector. The  $\mathbf{u}_9$  vector is linear in  $\zeta$  as shown below:

$$\mathbf{u}_9 = \mathbf{u}_0 + \zeta \frac{t}{2} \mathbf{u}_1 = \sum_{i=1}^9 N_i(\xi, \eta) (\mathbf{u}_0)_i + \zeta \sum_{i=1}^9 N_i(\xi, \eta) \left(\frac{t}{2} \mathbf{u}_1\right)_i \quad (3)$$

In contrast to the traditional degenerated solid shell, no rotational angles are used in this approach.

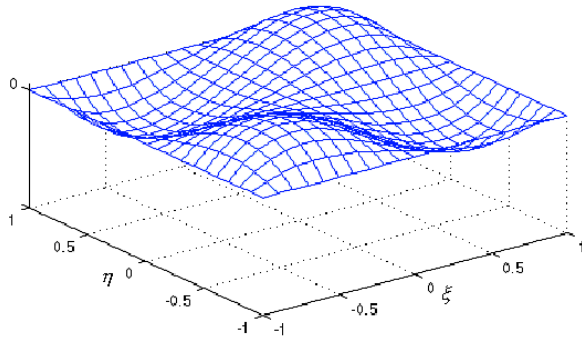


Figure 2 : Bubble function displacement

## 2.2 Bubble Function Displacement

A bubble function is a polynomial function that disappears along the element boundaries and at all nodal points. For finite element formulations, it is desirable to keep the order of the bubble function as low as possible. For this study, a single bubble function shown below is added to the nine-node assumed displacement field.

$$N_b(\xi, \eta) = \xi\eta(1 - \xi^2)(1 - \eta^2) \quad (4)$$

Figure 2 shows the bubble function in equation (4) in graphical form. The  $\mathbf{u}_b$  vector in equation (2) is also linear in  $\zeta$  as shown below:

$$\mathbf{u}_b = \mathbf{u}_{b_0} + \zeta \mathbf{u}_{b_1} \quad (5)$$

With the introduction of the above bubble function, the  $\mathbf{u}_{b_0}$  and  $\mathbf{u}_{b_1}$  vectors can be expressed as:

$$\begin{aligned} \mathbf{u}_{b_0} &= N_b(\xi, \eta) \mathbf{a} \\ \mathbf{u}_{b_1} &= N_b(\xi, \eta) \mathbf{b} \end{aligned} \quad (6)$$

where the parameters  $\mathbf{a}$  and  $\mathbf{b}$  are the internal degrees of freedom, which can be eliminated at the element level by static condensation.

## 2.3 Assumed Strain Field

The assumed strain formulation can provide an effective means of alleviating element locking while maintaining kinematic stability. The selection of a proper assumed strain field is vital to the element performance. For the present element, the assumed strain vector can be divided into three parts as

$$\boldsymbol{\varepsilon} = \boldsymbol{\varepsilon}^L + \boldsymbol{\varepsilon}^H + \boldsymbol{\varepsilon}^B \quad (7)$$

The  $\boldsymbol{\varepsilon}^L$  part is bilinear in  $\xi$  and  $\eta$  as shown below.

$$\begin{aligned} \varepsilon_{xx}^L &= \alpha_1 + \alpha_2 \xi + \alpha_3 \eta + \alpha_4 \xi \eta + (\alpha_{25} + \alpha_{26} \xi + \alpha_{27} \eta + \alpha_{28} \xi \eta) \zeta \\ \varepsilon_{yy}^L &= \alpha_5 + \alpha_6 \xi + \alpha_7 \eta + \alpha_8 \xi \eta + (\alpha_{29} + \alpha_{30} \xi + \alpha_{31} \eta + \alpha_{32} \xi \eta) \zeta \\ \varepsilon_{zz}^L &= \alpha_9 + \alpha_{10} \xi + \alpha_{11} \eta + \alpha_{12} \xi \eta \\ \varepsilon_{xy}^L &= \alpha_{13} + \alpha_{14} \xi + \alpha_{15} \eta + \alpha_{16} \xi \eta + (\alpha_{33} + \alpha_{34} \xi + \alpha_{35} \eta + \alpha_{36} \xi \eta) \zeta \\ \varepsilon_{yz}^L &= \alpha_{17} + \alpha_{18} \xi + \alpha_{19} \eta + \alpha_{20} \xi \eta + (\alpha_{37} + \alpha_{38} \xi + \alpha_{39} \eta + \alpha_{40} \xi \eta) \zeta \\ \varepsilon_{zx}^L &= \alpha_{21} + \alpha_{22} \xi + \alpha_{23} \eta + \alpha_{24} \xi \eta + (\alpha_{41} + \alpha_{42} \xi + \alpha_{43} \eta + \alpha_{44} \xi \eta) \zeta \end{aligned} \quad (8)$$

The second part,  $\boldsymbol{\varepsilon}^H$ , in equation (7) is chosen as follows:

$$\begin{aligned} \varepsilon_{xx}^L &= \alpha_{45} \xi \eta^2 + \alpha_{48} \xi \eta^2 \zeta \\ \varepsilon_{yy}^L &= \alpha_{46} \xi^2 \eta + \alpha_{49} \xi^2 \eta \zeta \\ \varepsilon_{zz}^L &= 0 \\ \varepsilon_{xy}^L &= 0 \\ \varepsilon_{yz}^L &= \alpha_{47} \xi^2 \eta + \alpha_{50} \xi^2 \eta \zeta \\ \varepsilon_{zx}^L &= \alpha_{47} \xi \eta^2 + \alpha_{50} \xi \eta^2 \zeta \end{aligned} \quad (9)$$

The above strain field with  $\boldsymbol{\varepsilon}^L$  and  $\boldsymbol{\varepsilon}^H$  is identical to that previously used for the formulation of a nine-node element with no bubble function displacement.

For the selection of  $\boldsymbol{\epsilon}^B$ , let's consider the six displacement modes with coefficients  $a_i$  and  $b_i$ , corresponding to the bubble function displacement vectors in equation (6), as follows:

$$\begin{aligned} u_{b_0} &= a_1 \cdot \xi \eta (1 - \xi^2) (1 - \eta^2) \\ v_{b_0} &= a_2 \cdot \xi \eta (1 - \xi^2) (1 - \eta^2) \\ w_{b_0} &= a_3 \cdot \xi \eta (1 - \xi^2) (1 - \eta^2) \\ u_{b_1} &= b_1 \cdot \xi \eta (1 - \xi^2) (1 - \eta^2) \\ v_{b_1} &= b_2 \cdot \xi \eta (1 - \xi^2) (1 - \eta^2) \\ w_{b_1} &= b_3 \cdot \xi \eta (1 - \xi^2) (1 - \eta^2) \end{aligned} \quad (10)$$

For a flat rectangular element with sides along  $x = \pm 1$  and  $y = \pm 1$ , the geometrically linear strain components corresponding to the above displacements are expressed as

$$\begin{aligned} \bar{\epsilon}_{xx} &= a_1(\eta - 3\xi^2\eta - \eta^3 + 3\xi^2\eta^3) + \zeta \cdot b_1(\eta - 3\xi^2\eta - \eta^3 + 3\xi^2\eta^3) \\ \bar{\epsilon}_{yy} &= a_2(\xi - 3\xi\eta^2 - \xi^3 + 3\xi^3\eta^2) + \zeta \cdot b_2(\xi - 3\xi\eta^2 - \xi^3 + 3\xi^3\eta^2) \\ \bar{\epsilon}_{zz} &= b_3(\xi\eta - \xi^3\eta - \xi\eta^3 + \xi^3\eta^3) \\ \bar{\epsilon}_{xy} &= a_1(\xi - 3\xi\eta^2 - \xi^3 + 3\xi^3\eta^2) + a_2(\eta - 3\xi^2\eta - \eta^3 + 3\xi^2\eta^3) \\ &\quad + \zeta \cdot b_1(\xi - 3\xi\eta^2 - \xi^3 + 3\xi^3\eta^2) \\ &\quad + \zeta \cdot b_2(\eta - 3\xi^2\eta - \eta^3 + 3\xi^2\eta^3) \\ \bar{\epsilon}_{yz} &= a_3(\xi - 3\xi\eta^2 - \xi^3 + 3\xi^3\eta^2) + b_2(\xi\eta - \xi^3\eta - \xi\eta^3 + \xi^3\eta^3) \\ &\quad + \zeta \cdot b_3(\xi - 3\xi\eta^2 - \xi^3 + 3\xi^3\eta^2) \\ \bar{\epsilon}_{zx} &= a_3(\eta - 3\xi^2\eta - \eta^3 + 3\xi^2\eta^3) + b_1(\xi\eta - \xi^3\eta - \xi\eta^3 + \xi^3\eta^3) \\ &\quad + \zeta \cdot b_3(\eta - 3\xi^2\eta - \eta^3 + 3\xi^2\eta^3) \end{aligned} \quad (11)$$

The selection of  $\boldsymbol{\epsilon}^B$  is based on the displacement-dependent strain field in equation (11). To alleviate element locking, the assumed strain field needs to be as simple as possible, without triggering undesirable spurious kinematic modes. This requirement can be met by choosing only one term for each displacement mode,  $a_i$  and  $b_i$  in the  $\zeta$ -independent part in equation (11). In the present formulation, an assumed strain field  $\boldsymbol{\epsilon}^B$  is selected

as follows:

$$\begin{aligned} \epsilon_{xx}^B &= \alpha_{51}(-3\xi^2\eta - \eta^3 + 3\xi^2\eta^3) + \alpha_{55}(-3\xi^2\eta - \eta^3 + 3\xi^2\eta^3)\zeta \\ \epsilon_{yy}^B &= \alpha_{52}(-3\xi\eta^2 - \xi^3 + 3\xi^3\eta^2) + \alpha_{56}(-3\xi\eta^2 - \xi^3 + 3\xi^3\eta^2)\zeta \\ \epsilon_{zz}^B &= \alpha_{53}(-\xi^3\eta - \xi\eta^3 + \xi^3\eta^3) \\ \epsilon_{xy}^B &= 0 \\ \epsilon_{yz}^B &= \alpha_{54}(-3\xi\eta^2 - \xi^3 + 3\xi^3\eta^2) + \alpha_{56}(-\xi^3\eta - \xi\eta^3 + \xi^3\eta^3) \\ \epsilon_{zx}^B &= \alpha_{54}(-3\xi^2\eta - \eta^3 + 3\xi^2\eta^3) + \alpha_{55}(-\xi^3\eta - \xi\eta^3 + \xi^3\eta^3) \end{aligned} \quad (12)$$

The bilinear terms are excluded because they are present in  $\boldsymbol{\epsilon}^L$ . There are no additional terms in  $\epsilon_{xy}^B$  because  $a_1$ ,  $a_2$ ,  $b_1$ , and  $b_2$  modes are present in  $\epsilon_{xx}^B$  and  $\epsilon_{yy}^B$ . The assumed strain field has 56 strain parameters. It turns out that the element exhibits two spurious kinematic modes, when the current choice of assumed strain field is used. However, they are incompatible and disappear when only two elements are assembled.

Although the selection of the assumed strain field is carried out over a flat rectangular element, the same assumed strain field is used for a curved element using a local coordinate system, in which the  $z$ -axis is normal to the mid-surface and the  $x$  and  $y$  axes are tangent to the surface.

It is also noted that the assumed strain field is neither complete nor symmetric in  $\xi$  and  $\eta$ . Accordingly, a specially defined local coordinate system is introduced to maintain element invariance [Park and Lee (1995)].

The construction of the local coordinate system can be summarized as follows. A reference local coordinate system is defined at the center of the element mid-surface ( $\xi = \eta = \zeta = 0$ ). First, unit vectors  $\mathbf{a}_\xi$  and  $\mathbf{a}_\eta$ , parallel to parental coordinates  $\xi$  and  $\eta$ , and a unit vector,  $\mathbf{v}_3^C$  normal to the mid-surface are defined as

$$\begin{aligned} \mathbf{a}_\xi &= \frac{\partial \mathbf{x}_0}{\partial \xi} / \left| \frac{\partial \mathbf{x}_0}{\partial \xi} \right| \\ \mathbf{a}_\eta &= \frac{\partial \mathbf{x}_0}{\partial \eta} / \left| \frac{\partial \mathbf{x}_0}{\partial \eta} \right| \\ \mathbf{v}_3^C &= \mathbf{a}_\xi \times \mathbf{a}_\eta \end{aligned} \quad (13)$$

where  $\mathbf{x}_0$  is the position vector of a point on the mid-surface as shown in equation (1). Then,  $\mathbf{v}_m$ , a unit vector bisecting  $\mathbf{a}_\xi$  and  $\mathbf{a}_\eta$ , is formed as shown in Fig. 3. A unit vector  $\mathbf{v}_1^C$  of the local coordinate system is constructed

by bisecting  $\mathbf{v}_m$  and  $\mathbf{v}_m \times \mathbf{v}_3^C$ , and  $\mathbf{v}_2^C$  is defined by taking cross product of  $\mathbf{v}_3^C$  and  $\mathbf{v}_1^C$ . This completes the construction of the unit vectors for the local coordinate system at the element center. The local coordinate system at an integration point other than the element center is determined by rotating the  $\mathbf{v}_3^C$  vector to a unit vector that is normal to the surface at the point.

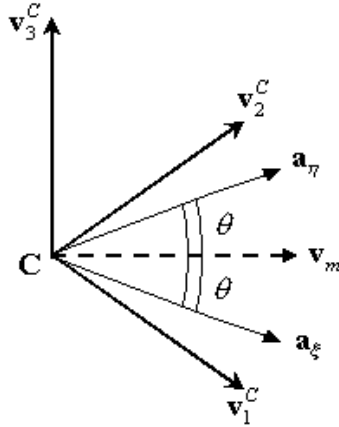


**Figure 3** : The local coordinate system at the element center

### 2.4 Compatibility and Equilibrium

The independently assumed strain and the displacement-dependent strain can be related through the compatibility equation expressed as:

$$\int_V \delta \boldsymbol{\epsilon}^T \mathbf{C}_e (\bar{\boldsymbol{\epsilon}} - \boldsymbol{\epsilon}) dV = 0 \quad (14)$$

where  $\delta \boldsymbol{\epsilon}$  is a virtual independent strain vector and  $\mathbf{C}_e$  is the matrix of linear elastic stiffness constants.

For a solid in equilibrium,

$$\int_V \delta \bar{\boldsymbol{\epsilon}}^T \boldsymbol{\sigma} dV - \delta W = 0 \quad (15)$$

where  $\boldsymbol{\sigma}$  is the second Piola-Kirchhoff stress vector,  $\delta \bar{\boldsymbol{\epsilon}}$  is the virtual displacement-dependent strain vector,  $\delta W$  is the virtual work due to the applied load and  $V$  represents the volume of the original configuration. Equilibrium is satisfied over the deformed configuration. The stress vector is related to the independent strain vector as

$$\boldsymbol{\sigma} = \mathbf{C}_e \boldsymbol{\epsilon} \quad (16)$$

In the solid shell element formulation, strains, virtual strains, and the determinant  $J$  of the Jacobian matrix are assumed to be linear in  $\zeta$  such that

$$\begin{aligned} \bar{\boldsymbol{\epsilon}} &= \bar{\boldsymbol{\epsilon}}_0 + \zeta \cdot \bar{\boldsymbol{\epsilon}}_1 & \delta \bar{\boldsymbol{\epsilon}} &= \delta \bar{\boldsymbol{\epsilon}}_0 + \zeta \cdot \delta \bar{\boldsymbol{\epsilon}}_1 \\ \boldsymbol{\epsilon} &= \boldsymbol{\epsilon}_0 + \zeta \cdot \boldsymbol{\epsilon}_1 & \delta \boldsymbol{\epsilon} &= \delta \boldsymbol{\epsilon}_0 + \zeta \cdot \delta \boldsymbol{\epsilon}_1 \end{aligned} \quad (17)$$

$$J = J_0(\xi, \eta) + \zeta \cdot J_1(\xi, \eta_0)$$

The assumptions in equation (17) allow analytical integration through the shell thickness. This feature is convenient for modeling of laminated composite structures [Kim and Lee (1988)]. The finite element equilibrium equation involving the tangent stiffness matrix vector and the incremental load vector is obtained via the procedure described by Park, Cho and Lee (1995). The degrees of freedom (DOF) vector corresponding to the bubble function displacement is statically condensed out at element level to maintain the number of element DOF at 54. If desired, the DOF at the center node can also be statically condensed out to construct an eight-node element with 48 DOF. It should be noted that, due to the bubble functions in the assumed displacement field and the additional higher order terms in the assumed strain field, the  $4 \times 4$  point Gaussian quadrature rule is needed over the  $\xi, \eta$  plane for generation of the element stiffness matrix. This is in contrast to the  $3 \times 3$  point rule needed for the existing nine-node assumed strain solid shell element with no bubble functions.

### 3 Numerical Tests

Several numerical tests are conducted to examine the performance of the new solid shell element in comparison with that of the existing nine-node solid shell element. Examples chosen are geometrically linear and nonlinear plates and shells of simple geometries under static loading conditions. First, the effect of increase in the number of integration points on the computational efficiency of the current approach is tested. Secondly, numerical tests involving plates and shells modeled with uniform meshes are conducted to confirm that the newly added assumed strain terms in conjunction with the bubble function displacement do not reintroduce element locking. As one of the examples, the result for a geometrically nonlinear analysis of a pinched ring, is presented in the following. Subsequently, geometrically nonlinear analyses of a thin plate and a hemisphere, modeled with uniform meshes and non-uniform meshes, are carried out to compare the

performance of the new element with the existing element. For convenience of presenting numerical results, the following designations are used for the new element and the existing element.

SHELL9B: Nine-node assumed strain solid shell element with bubble function displacements

SHELL9: Nine-node assumed strain solid shell element [Kim and Lee (1988), Park, Cho, and Lee (1995)]

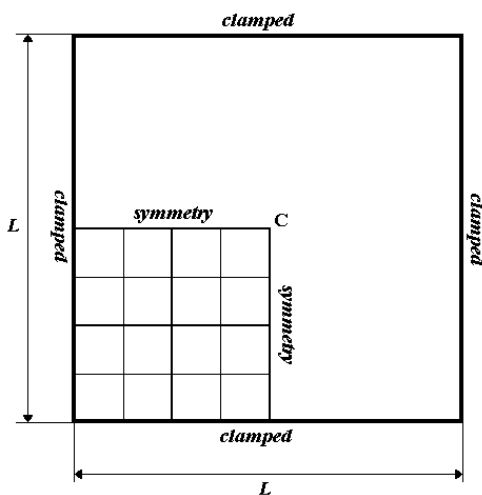


Figure 4 : A square plate

### 3.1 The Number of Integration Points

In order to investigate the effect of the number of integration points on computing time, a test is conducted in which the stiffness matrix of a single element is computed 100 times consecutively. Numerical results show that the computing (elapsed) time for SHELL9B is 1.8 times of that for SHELL9. Subsequently, a square plate, clamped on all edges and loaded at the center point C as shown in Fig. 4, is considered to investigate the effect as a problem size grows. Due to the geometric and load symmetry, only one quarter of the plate is modeled using a 2x2, 4x4, 8x8, 16x16, and 32x32 meshes. In Fig. 5, the ratio of elapsed time for a geometrically linear analysis using SHELL9B, normalized with respect to the time for SHELL9, is plotted against the number of elements in one direction. It shows that, as the problem size grows, the ratio of elapsed time between SHELL9B and SHELL9 approaches unity.

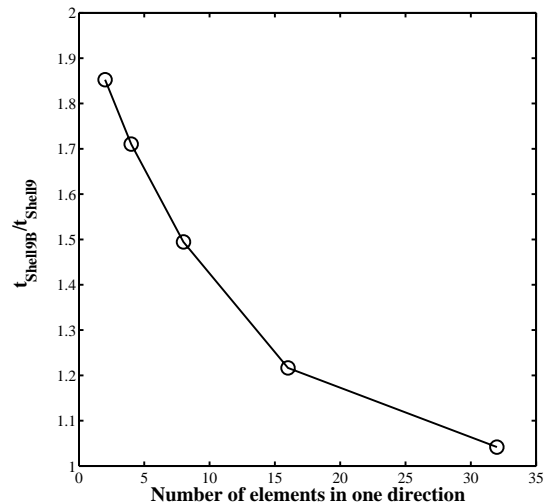


Figure 5 : Time vs. number of elements in one direction

### 3.2 A Pinched Ring

A circular ring, subjected to two opposite line loads, as shown in Fig. 6, serves as a simple example problem to examine the membrane locking of curved shell elements.

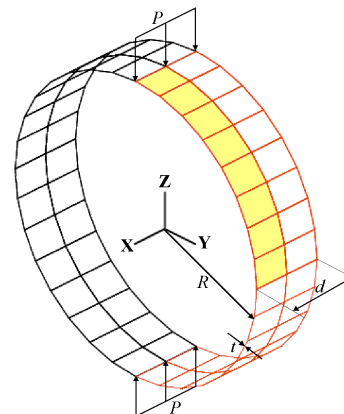


Figure 6 : A pinched ring

The radius  $R$  of the ring is 100" and the width  $d$  is 1". The ring material is isotropic with a Young's modulus  $E = 1 \times 10^7$  psi and a Poisson's ratio  $\nu = 0.3$ . Due to the symmetry in geometry and loading conditions, only one quarter in the circumferential direction and one half in the width direction is modeled with a 1x4 uniform mesh. A geometrically nonlinear analysis is conducted for three different radius-to-thickness ratios of  $R/t = 100, 500,$  and 1000. A deformed shape of the pinched ring with  $R/t = 100$  is shown in Fig. 7. Figures 8-10 shows the displace-

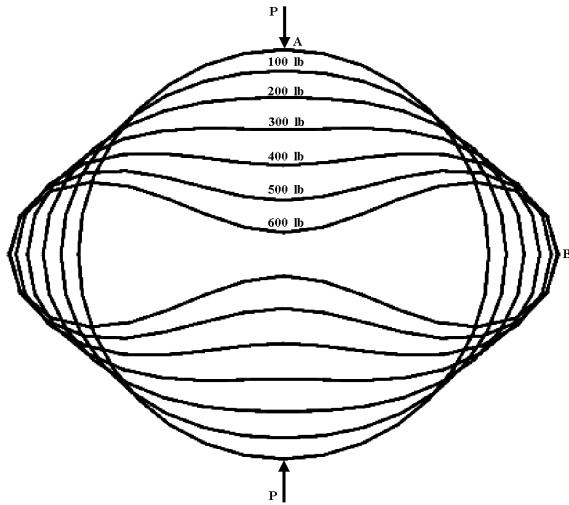


Figure 7 : Deformed shape of a pinched ring with  $R/t = 100$

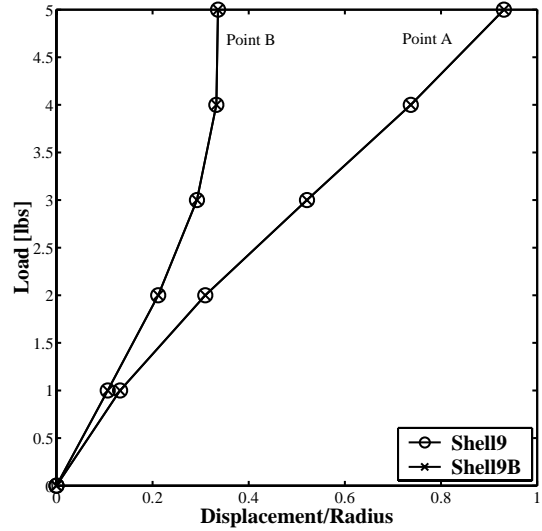


Figure 9 : Load vs. displacement of a geometrically nonlinear pinched ring with  $R/t = 500$

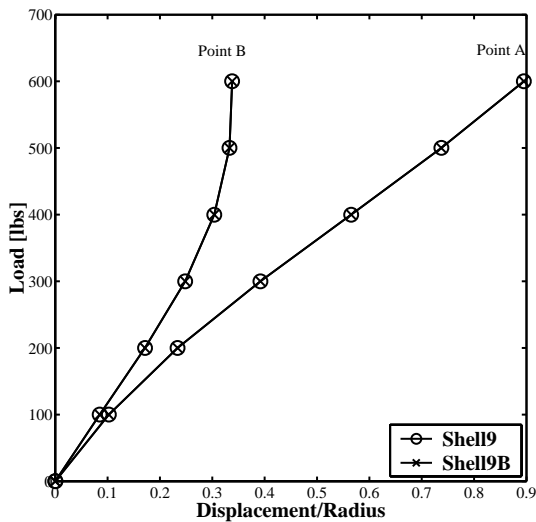


Figure 8 : Load vs. displacement of a geometrically nonlinear pinched ring with  $R/t = 100$

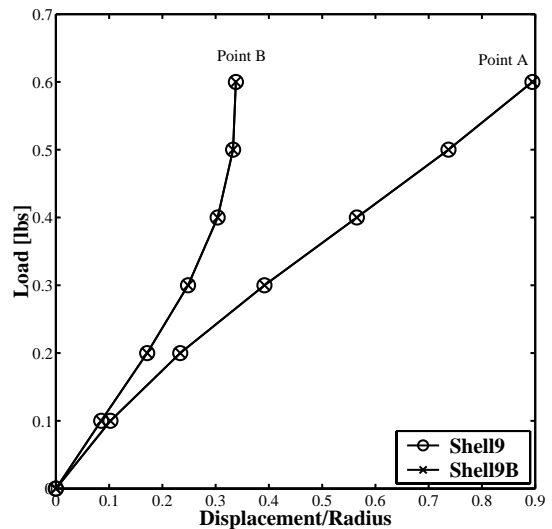


Figure 10 : Load vs. displacement of a geometrically nonlinear pinched ring with  $R/t = 1000$

ment in the direction normal to the surface at two points. As shown in these figures, there is no difference between SHELL9 and SHELL9B solutions. Both elements perform well, exhibiting no signs of element locking.

### 3.3 A Thin Square Plate Under a Point Load

A square plate, clamped on all edges and loaded at the center point C, as shown in Fig. 4 is revisited.

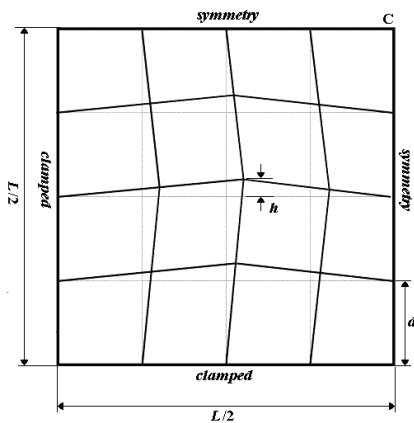


Figure 11 : A square plate (2x2 mesh)

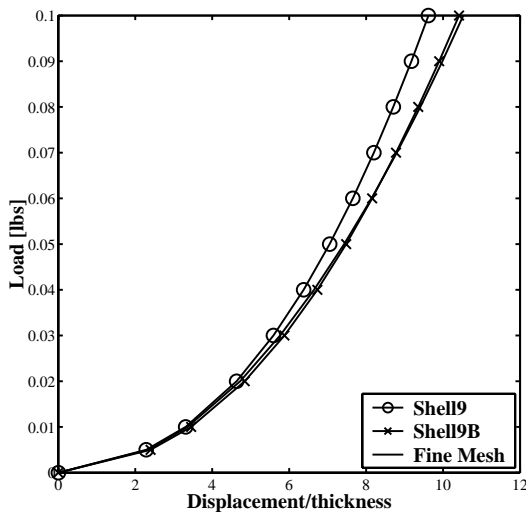


Figure 12 : Load vs. displacement of a clamped plate with distorted mesh,  $L/t=1000$

The length  $L$  of the plate is 2" and the thickness is 0.002". The material is isotropic with a Young's modulus  $E = 1.7472 \times 10^7$  psi and a Poisson's ratio  $\nu = 0.3$ . Due to the geometric and load symmetry, only one quarter of the plate is modeled using a 2x2 mesh. To examine the effect

of mesh distortion on the element performance, the plate is modeled with the distorted mesh as shown in Fig. 11. The degree of the distortion is represented by  $d/h = 0.2$ . Numerical solutions obtained by the geometrically linear analysis are 88.1% (SHELL9) and 99.1% (Shell9B) of the analytical solution. The results of the geometrically non-linear analysis are shown in Fig. 12 where the solution obtained by an 8x8 uniform mesh (Fine Mesh) is used as the reference. SHELL9B outperforms SHELL9 as the load increases.

### 3.4 A Hemisphere with Alternating Point Loads

A hemispherical shell with an 18-degree hole at the top is under alternating point loads as shown in Fig. 13.

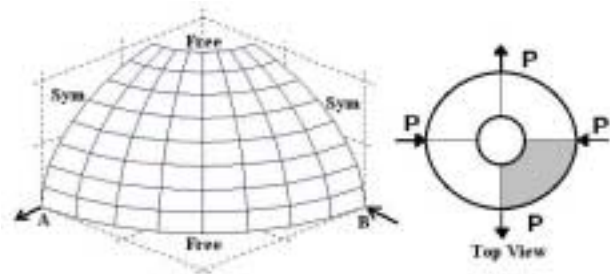


Figure 13 : A hemisphere with a hole at the top

The radius  $R$  of the hemisphere is 10" and the thickness  $t$  is 0.01". The material is isotropic with a Young's modulus  $E = 6.825 \times 10^7$  psi and a Poisson's ratio  $\nu = 0.3$ . Due to the geometric and loading symmetry, only one quarter of the hemisphere, the shaded area from the top view in Fig. 13 is modeled using various distorted meshes. As an example, an 8x8 distorted mesh is shown in Fig. 14. The normal displacements obtained with a 16x16 uniform mesh are used as a reference. The 'uniform' mesh is obtained by equally dividing the angles in the meridian and latitude directions.

Geometrically linear analyses for the hemisphere model are conducted using the 2x2, 4x4, 6x6, and 8x8 distorted meshes. Figures 15 and 16 show the displacement in the loading direction, normalized to the 16x16 uniform mesh solution. The results for the two different radius-to-thickness ratios,  $R/t=250$  and  $R/t=1000$ , demonstrate that SHELL9B outperforms SHELL9 when coarse meshes are used.

Subsequently, geometrically nonlinear analyses are conducted for two different models. In Figs. 17 and 18, the

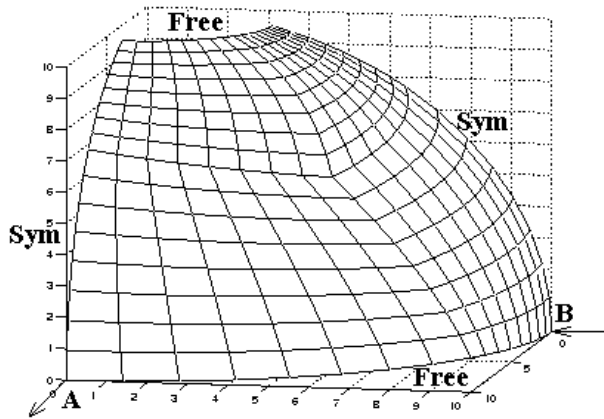


Figure 14 : A hemisphere model with distorted mesh

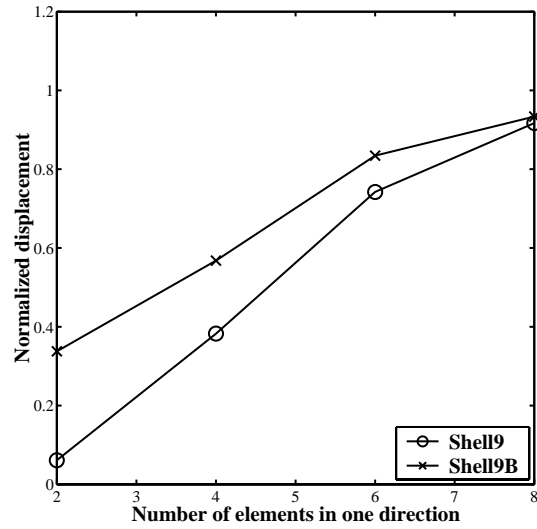


Figure 16 : Displacement at a load point vs. number of elements in one direction,  $R/t=1000$

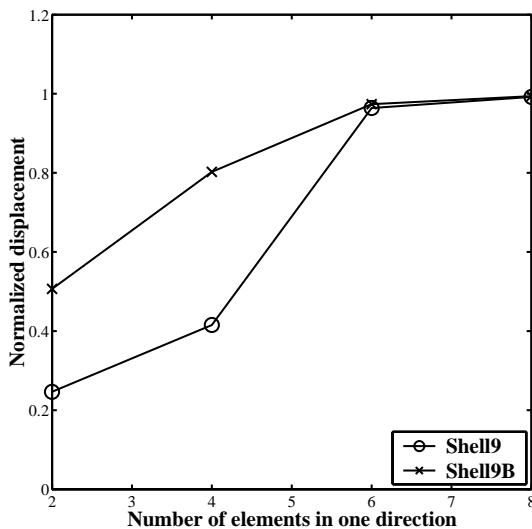


Figure 15 : Displacement at a load point vs. number of elements in one direction,  $R/t=250$

displacements at the load point A and B are plotted along with the Fine Mesh solution obtained using a  $16 \times 16$  uniform mesh. For the uniform mesh ( $4 \times 4$ ) case, SHELL9B outperforms SHELL9 as load increases. For the distorted mesh ( $8 \times 8$ ) case shown in Fig. 18, SHELL9B is significantly less sensitive to mesh distortion as the load increases. The results demonstrate that SHELL9B outperforms SHELL9 for both cases.

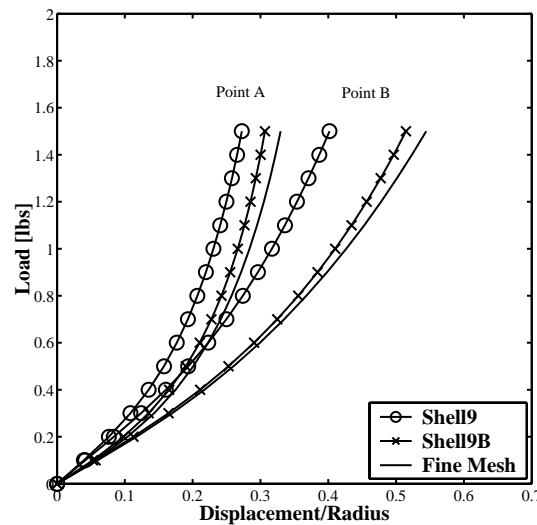
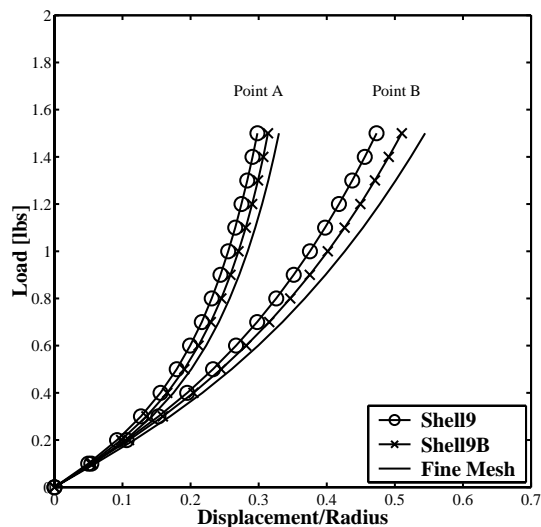


Figure 17 : Load vs. displacement of a geometrically nonlinear hemisphere with  $R/t=1000$ : ( $4 \times 4$  uniform mesh)



**Figure 18** : Load vs. displacement of a geometrically nonlinear hemisphere with  $R/t=1000$ : (8x8 distorted mesh)

#### 4 Conclusions

The results of numerical tests, conducted on geometrically linear and nonlinear plates and shells, show the effectiveness of the newly developed solid shell element. For finite element models with non-uniform meshes, the new element is significantly less sensitive to mesh distortion than the existing nine-node solid shell element. The improved performance of this new element demonstrates the effectiveness of the present formulation that combines the simplest bubble function displacement with a carefully selected assumed strain field.

#### References

- Ahmad, S., Irons, B. M. and Zienkiewicz, O. C.** (1970): Analysis of thick and thin shell structures by curved elements, *Int. J. Numer. Meth. Engng*, Vol. 2, pp. 419-451
- Andelfinger, U. and Ramm, E.** (1993): EAS-element for two-dimensional, three-dimensional, plate and shell structures and their equivalence to HR-elements, *Int. J. Numer. Meth. Engng*, Vol. 36, 1993, pp. 1311-1337
- Ausserer, M. F. and Lee, S. W.** (1988): An eighteen node solid element for thin shell analysis, *Int. J. Numer. Meth. Engng*, Vol. 26, pp. 1345-1364
- Betsch, P. and Stein, E.** (1995): An assumed strain approach avoiding artificial thickness straining for a non-

linear 4-node shell element, *Comm. Numer. Methods Eng.*, Vol. 11, pp. 899-909

**Buchter, N., Ramm, E. and Roehl, D.** (1994): Three-dimensional extension of nonlinear shell formulation based on the enhanced assumed strain concept, *Int. J. Numer. Meth. Engng*, Vol. 37, pp. 2551-2568

**Cho, C. Y. and Atluri, S. N.** (2001): Analysis of shear-flexible beams, using the meshless local Petrov-Galerkin method, based on a locking-free formulation, *Engineering Computations*, Vol. 18, No. 1 & 2, pp. 215-240

**Cho, J. Y., Kim, H. G., and Atluri, S. N.** (1999): Analysis of thin beams using the meshless local Petrov-Galerkin method With generalized moving least square interpolations, *CMES: Computer Modeling in Engineering & Sciences*, Vol. 24, No. 5, pp. 334-347

**El-Zafrany, A.** (2001): Boundary element stress analysis of thick Reissner plates in bending under generalized loading, *CMES: Computer Modeling in Engineering & Sciences*, Vol. 2, No. 1, pp. 27-38

**Gu, Y.T. and Liu, G.R.,** (2001): A meshless local Petrov-Galerkin (MLPG) formulation for static and free vibration analyses of thin plates, *CMES: Computer Modeling in Engineering & Sciences*, Vol. 2, No. 4, pp. 463-476

**Hong, W., Kim, Y.H., and Lee, S.W.** (2001): Assumed strain triangular solid shell elements with bubble function displacements for analysis of plates and shells, *Int. J. Numer. Meth. Engng*, Vol. 52, no. 4, pp. 455-469

**Hong, W., Kim, Y.H., and Lee, S.W.** (2001): An assumed strain triangular curved solid shell element formulation for analysis of plates and shells undergoing finite rotation, *Int. J. Numer. Meth. Engng*, Vol.52, No. 7, pp.747-761

**Kemp, B., Cho, C. and Lee, S. W.** (1998): A four-node solid shell element formulation with assumed strain, *Int. J. Numer. Meth. Engng*, Vol. 43, pp. 909-924

**Kim, J.H., Kim, Y.H. and Lee, S.W.** (2000): An assumed strain formulation of efficient solid triangular element for general shell analysis, *Int. J. Numer. Meth. Engng*, Vol. 47, no. 8, pp. 1481-1497

**Kim, Y. H. and Lee, S. W.** (1988): A solid element formulation for large deflection analysis of composite shell structures, *Computers and Structures*, Vol. 30, pp. 269-274

**Lee, S. W. and Pian, T. H. H.** (1978): Improvement

of plate and shell finite element by mixed formulations, *AIAA Journal*, Vol. 16, pp. 29-34

**Park, H. C., Cho, C. M. and Lee, S. W.** (1995): An efficient assumed strain element model with six DOF per node for geometrically nonlinear shells, *Int. J. Numer. Meth. Engng*, Vol. 38, pp. 4101-4122

**Park, H. C. and Lee, S. W.** (1995): A local coordinate system for assumed strain shell element formulation, *Computational Mechanics*, Vol. 15, No. 5, pp. 473-484

**Pinsky, P. M. and Jasti, R. V.** (1989): A mixed finite element formulation for Reissner-Mindlin plates based on the use of bubble functions, *Int. J. Numer. Meth. Engng*, Vol. 28, pp. 1677-1702

**Rhiu, J.J. and Lee, S.W.** (1987): A new efficient mixed formulation for thin shell finite element model, *Int. J. Numer. Meth. Engng*, Vol. 24, pp. 581-604

**Rhiu, J. J., Russell, R. M. and Lee, S. W.** (1990): Two higher-order shell finite elements with stabilization matrix, *AIAA Journal*, Vol. 28, pp. 1517-1524

**Saleeb, A. F., Chang, T. Y., Graf, W. and Yingyeunyoung S.** (1990): A hybrid/mixed model for nonlinear shell analysis and its applications to large-rotation problems, *Int. J. Numer. Meth. Engng*, Vol. 29, 1990, pp. 407-446

**Simo, J.C. and Rifai, M.S.** (1990): On a stress resultant geometrically exact shell model. part III: computational aspects of the nonlinear theory, *Comp. Meth. Appl. Mech. Eng.*, Vol. 79, pp. 21-70

**Simo, J. C., Rifai, M. S. and Fox, D. D.** (1990): On a stress resultant geometrically exact shell model. part IV: variable thickness shells with through-the-thickness stretching, *Comp. Meth. Appl. Mech. Eng.*, Vol. 81, 1990, pp. 91-126

**Yang, H. T. Y., Saigal, S., Masoud, A., and Kapania, R. K.** (2000): A survey of recent shell finite elements, *Int. J. Numer. Meth. Engng*, Vol. 47, 2000, pp. 101-127

**Yeom, C.H. and Lee, S.W.** (1989): An assumed strain element model for large deflection composite shells, *Int. J. Numer. Meth. Engng*, Vol. 28, pp. 1749-1768

